Journal of Materials Chemistry A

Accepted Manuscript

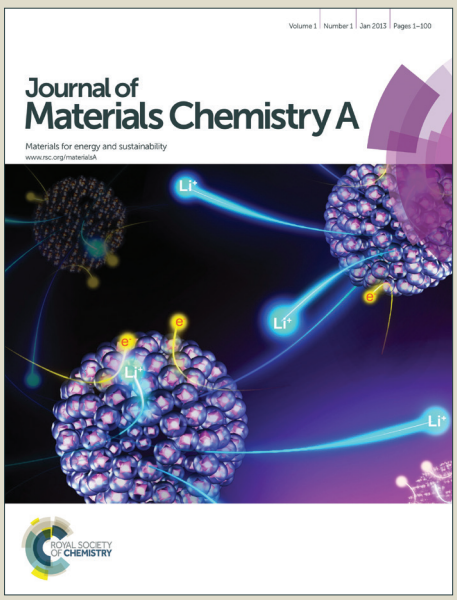

ROYAL SOCIETY OF CHEMISTRY

www.rsc.org/materialsA

Influence of Mono Versus Bis-Electron-Donor Ancillary Ligands in Heteroleptic Ru (II) Bipyridyl Complexes on the Electron Injection from the First Excited Singlet and Triplet States in Dye-sensitized Solar Cells

Hammad Cheema[a], Ashraful Islam[b], Liyuan Han[b], Bhoj Gautam[c] Robert Younts[c], Kenan Gundogdu[c], Ahmed El-Shafei[a]*

[a]Polymer and Color Chemistry Program, North Carolina State University, Raleigh, NC, 27695, USA

[b]Photovoltaic Materials Unit, National Institute for Materials Science, 1-2-1 Sengen, Tsukuba, Ibaraki 305-0047, Japan.

[c]Physics Department, North Carolina State University, Raleigh, NC, 27695, USA

*Corresponding author: Ahmed_El-Shafei@ncsu.edu

KEYWORDS: Dye-sensitized solar cells, mono vs. bis electron-donor ancillary ligand, solar-to-electric conversion, IPCE, Ru (II) bipyridyl complexes.

Abstract:

A novel heteroleptic Ru (II) bipyridyl complex (HD-1-mono) was molecularly designed with mono-carbazole ancillary ligand, synthesized and characterized for DSCs. The aim was to systematically study the influence of mono (HD-1-mono) versus bis-carbazole ancillary ligand (NCSU-10) on molar absorptivity, light harvesting efficiency (LHE), ground and excited state oxidation potentials, incident-photon-to-current conversion efficiency (IPCE), short-circuit photocurrent density (J_{sc}), and total solar-to-electric conversion efficiency (η) for DSCs. This study showed that HD-1-mono exhibited slightly lower V_{oc} but greater J_{sc} compared to NCSU-10. Though HD-1-mono showed lower extinction coefficient than NCSU-10, interestingly, it was

found that the decrease in molar extinction coefficient of HD-1-mono is not directly related to the short-circuit photocurrent density (J_{sc}). For example, HD-1-mono showed higher J_{sc} of 21.4 mA/cm^2 without the presence of any additives. However, under optimized conditions, HD-1-mono showed J_{sc} of 19.76 mA/cm^2, V_{oc} of 0.68V, with (%η) of 9.33 compared to J_{sc} of 19.58 mA/cm^2, V_{oc} of 0.71 and (%η) of 10.19 for NCSU-10, where N719 achieved J_{sc} of 16.85mA/cm^2, V_{oc} of 0.749V and (%η) of 9.32 under the same experimental device conditions. Impedance results for HD-1-mono showed shorter recombination time as compared to N719 and NCSU-10, which justify its lower V_{oc}. Femtosecond transient absorption spectroscopy results elucidated that electron injection from the first triplet state is 63% more efficient for HD-1-mono than that of NCSU-10.

1. Introduction

Dye-sensitized solar cells (DSCs) are unique compared to silicon-based solar cells in many ways. For examples, DSCs are made of inexpensive materials, their manufacturing is cost effective, flexible, can be made in different colors and exhibit superior performance in rainy, diffused and year around conditions [1-9]. Owing to the aforementioned unique features, different components of DSCs such as sensitizer, TiO_2 and redox shuttle have been widely studied and improved during the last two decades [7,8,10-13]. Sensitizer is one of the most critical component within a DSC and Ru (II) based sensitizers have continuously shown greater than 10% [5,14-18] over-all power conversion efficiency. Among the Ru (II) polypyridyl complexes N719 (11.18%) [19] is a popular benchmark dye in both academia and industry. However, strategies are needed to improve the NIR response of Ru (II) sensitizers, increase molar absorptivity and fine tuning of ground and excited state oxidation potentials. The goal is to molecularly engineer a panchromatic sensitizer which not only absorbs most of the energetic photons in the range of

400nm to 920nm but also maintains a favorable thermodynamic ground and excited states oxidation potentials for dye generation and electron injection, respectively, which would ultimately result in an ideal sensitizer with minimum recombination losses.

With the aforementioned in mind, this work is focused on the molecular modulations of a previously reported highly efficient Ru (II) based sensitizer known as NCSU-10 [5] as shown in Figure 1. Our strategy was to use one carbazole ancillary ligand, HD-1-mono (Figure 1), to reduce the molecular size and study how that influences the light harvesting efficiency, photovoltage, sensitizer redox properties, decay dynamics and the charge separation/recombinations at the dye/TiO_2/electrolyte interfaces. Similar ideas have been reported previously for sensitizers JK-56 [20] and D-20 [21]. In both cases mono-based sensitizers resulted in higher current and overall greater efficiency than the bis-ancillary ligand analogs due to decreased loading for bis analogs. However in both JK-56 and D-20, the ancillary ligands were of much larger molecular size compared to carbazole, thus molecular size is expected to have minimal influence in this study. To better understand the origin of higher J_{sc} in HD-1-mono compared to NCSU-10 and N719, TiO_2/dye interface properties were studied by impedance spectroscopy which is directly correlated to photocurrent and photovoltage. Time-correlated single photon counting (TCSPC) and ultra-fast transient absorption measurements were performed to understand the fundamental difference in the photo-physics and electron injection properties of HD-1-mono and NCSU-10 in solar cell form. UV-Vis, fluorescence, and cyclic voltammetry measurements were performed to ascertain the difference in molar absorptivity, excited state and redox properties of HD-1-mono and NCSU-10, respectively. The goal is to understand the fundamental difference between HD-1-mono and NCSU-10 for the design of more efficient sensitizers, both in terms of higher photocurrent and photovoltage for DSCs.

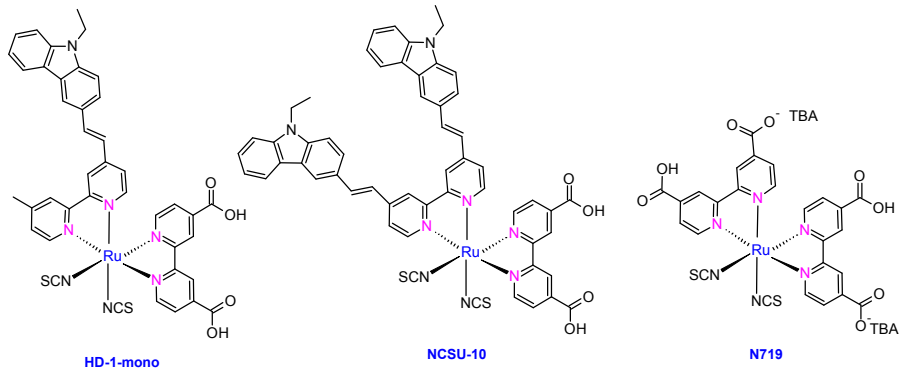

Figure 1. Molecular structures of complexes HD-1-mono, NCSU-10 and N719.

2. Results and Discussion

The synthesis of the proposed sensitizer HD-1-mono was carried out in a similar way as reported for NCSU-10 [5,22] using 1:1 molar ratio of 4,4'-dimethyl-2,2'-bipyridine to 9-ethyl-9H-carbazole-3-carbaldehyde. HD-1-mono was synthesized in the typical one-pot three-steps synthetic scheme as shown in SI. The typical raw product yield was up to 90%, which is then run through the Sephadex LH-20 column for three times to get the highly pure product in 55% yield.

2.1. Photopysical Measurements

A comparison between the UV-Vis absorption and emission spectra of N719, HD-1-mono, and NCSU-10 is given in Figure 2, and the results are summarized in Table 1.

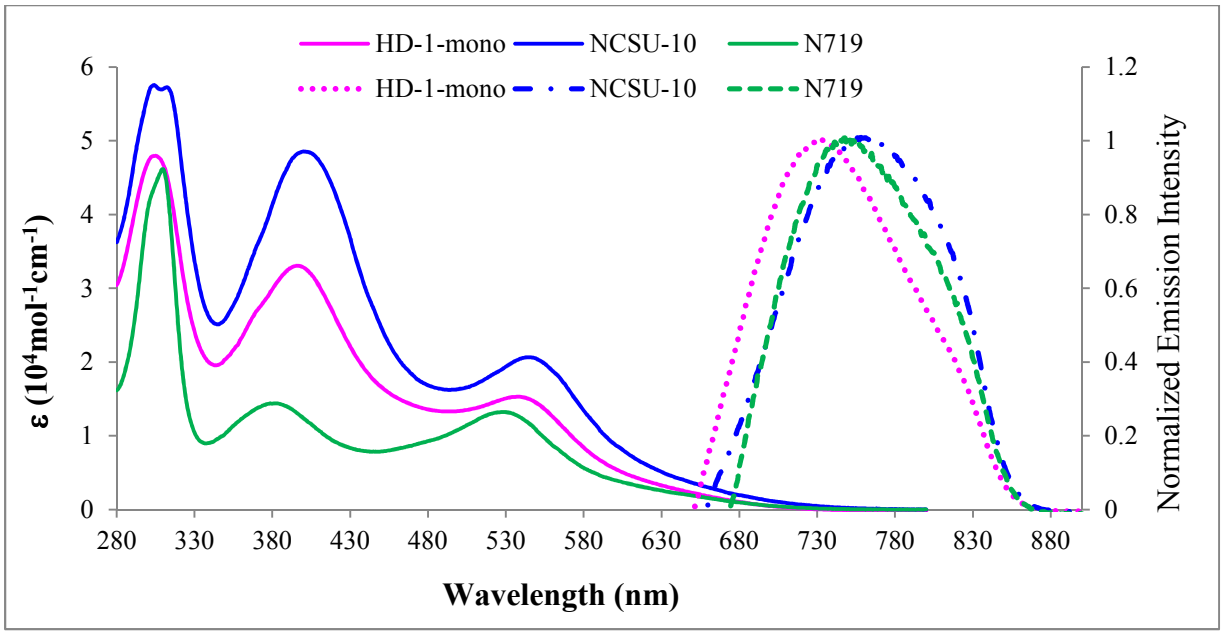

Figure 2. UV-Vis absorption (solid-line) and emission spectra (dashed-line) of complexes HD-1-mono as compared to N719 and NCSU-10 measured in DMF (2 x10-5M).

Table 1. Absorption and emission properties for HD-1-mono as compared to NCSU-10 and N719

Sensitizer	Absorption λ_{max} (nm)	ε (M^{-1} cm^{-1})	Emission λ_{max} (nm)
HD-1-mono	304,396, 538 (d→π*)	51,900;33,350; 15,550	728
NCSU-10	304, 401, 545 (d→π*)	57,550; 48,555; 20,650	758
N719	310,381, 529(d→π*)	46 100; 14 400; 12,800	744

Intense MLCT absorption peak was found for HD-1-mono at 538nm (15,550 $M^{-1}cm^{-1}$) compared to NCSU-10 at 545nm (20,650 $M^{-1}cm^{-1}$) and N719 at 529nm (12,800 $M^{-1}cm^{-1}$). HD-1-mono showed slightly blue shifted spectra and up to 30% decrease in extinction coefficient compared to NCSU-10. However, extended π-conjugation and stronger electron donating carbazole

ancillary ligand resulted in destabilized metal based HOMO (t_{2g}) and red shifted absorption spectra, compared to N719, due to decreased HOMO-LUMO gap, as shown in the energy level diagram of Figure 3. Emission λ_{max} for HD-1-mono was also blue shifted compared to that NCSU-10 and N719.

In terms of ancillary ligands itself, there was no substantial change in optical and electrochemical properties (SI Figure 8-10S) for HD-1-mono and NCSU-10, as observed by UV-Vis, emission and cyclic voltammetry. Thus molecular modulation of ancillary ligands was expected to have negligible effect on optical and electrochemical properties of the corresponding complexes.

2.2. Electrochemical Measurements

The ground state oxidation potential (GSOP) of HD-1-mono was measured in two ways. First, by cyclic voltammetry (CV) in solution form, and the second by a photoemission yield spectrometer (Riken Keiki AC-3E), while the dye anchored to TiO_2 film. The results are summarized and compared in Table 2. It was observed that while anchored to TiO_2, the GSOP of both dyes shifted negatively owing to de-protonation of complexes. CV graphs were used to calculate the oxidation onset which is equivalent to the GSOP (ground state oxidation potential) or HOMO level of the dye. Additionally, $E_{0\text{-}0}$ was calculated from the intersection point of experimental absorption and emission spectra and can be defined as the difference between the excited and ground state oxidation potentials. Then values of $E_{0\text{-}0}$ and GSOP were used to calculate the ESOP (excited state oxidation potential) or LUMO level of the dye, the values in volts (V) vs. NHE were converted to electron volt (eV) as shown in Equation 1.

$$ESOP = [(E_{0\text{-}0} + (GSOP\ (V) + 4.7)]\ eV \qquad \text{Equation (1)}$$

The GSOP value of -5.46 for HD-1-mono confirmed that the HOMO of this dye is below the I_3^-/I^- redox couple (-5.2 eV) [23], and the difference is large enough for electron replenishment and efficient dye regeneration. Additionally, the ESOP energy level of HD-1-mono was at -3.55eV which was above the conduction band edge of nanocrystalline TiO_2 (-4.2 eV)[24]. Similar measurements for NCSU-10 showed that GSOP is at -5.5eV and ESOP at -3.57eV thus resulting in favorable dye regeneration and electron injection, respectively. Thus owing to the energetically favorable excited states, the efficient electron injection into the CB edge of TiO_2 and dye regeneration was achieved with sensitizers HD-1-mono. According to the energy level diagram in Figure 3, the HOMO destabilization is in the order of HD-1-mono>NCSU-10>N719, which is consistent with the order of experimental J_{sc} of HD-1-mono>NCSU-10>N719.

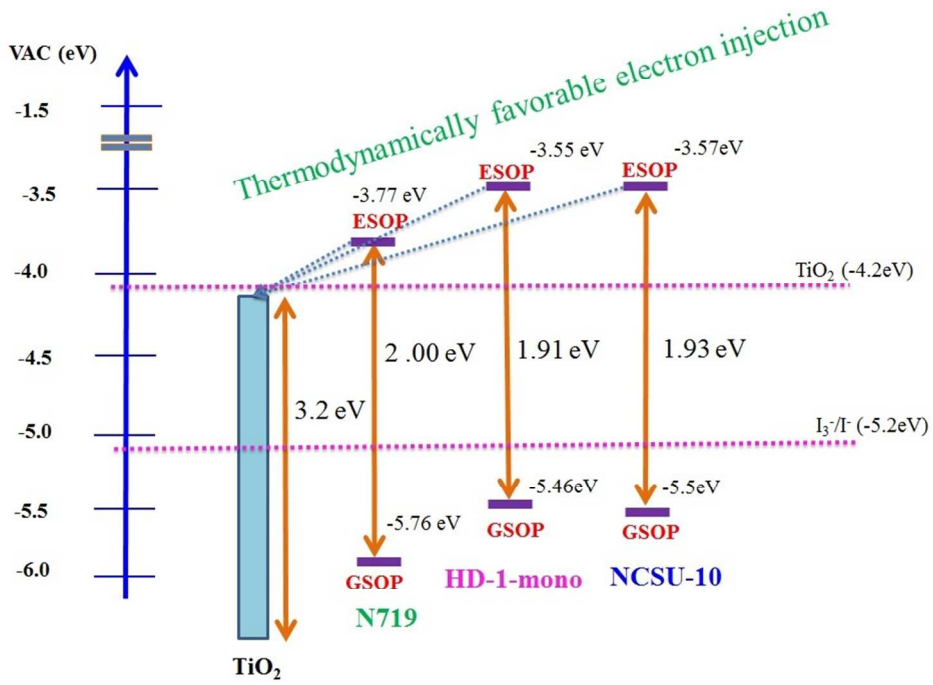

Figure 3. Energy level diagram and comparison between HOMO and LUMO of N719, HD-1-mono and NCSU-10

Table 2. Shows the excited state oxidation potential (E*), and the lowest singlet-singlet electronic transitions ($E_{0\text{-}0}$) for ligands and HD-1-mono compared to NCSU-10 and N719.

Sensitizer	Experimental (eV)			
	*$E_{0\text{-}0}$	♥GSOP(HOMO) (CV)	♥*GSOP(HOMO) (AC3)	E*
LH-1-mono	2.94	-5.65	--------	-2.71
L-NCSU-10	2.94	-5.66	--------	-2.72
HD-1-mono	1.91	-5.46	-5.38	-3.55
NCSU-10	1.93	-5.50	-5.50	-3.57
N719	1.99	-5.76	-5.76	-3.77

$E_{0\text{-}0}$= calculated from the intersection point of experimental absorption and emission spectra (DMF); ♥GSOP =ground state oxidation potential= E_{HOMO}; ♥GSOP was measured in DMF with 0.1 M [TBA][PF6] and with a scan rate of 50 mV s^{-1}. It was calibrated with Fc/Fc+ as internal reference and converted to NHE by addition of 0.63 V; ♥ GSOP was also measured using a photoemission yield spectrometer (Riken Keiki AC-3E); Excited-state oxidation potential, E* was calculated from: E* = GSOP + *$E_{0\text{-}0}$. Calculated GSOP, ESOP, and $E_{0\text{-}0}$ of N719 was performed elsewhere [5,25]. GSOP and ESOP for ligands were calculated using similar method as used for dyes.

Similar Ru (II) complexes have been recognized to have electron injection both from singlet and triplet energy states [8,26-28], thus it was important to estimate if the molecular modulation of the mono versus bis-ancillary ligands invoke direct changes in electron injection from singlet and triplet states and in their energy values. Singlet and triplet energy levels were estimated from the onset of fluorescence ($E_{0\text{-}0}$, Figure 2) and phosphorescence (SI Figure 13S) emission. It was found that HD-1-mono and NCSU-10 have singlet at 1.91eV, 1.93eV respectively and triplet energy levels at 1.36eV. Triplet energy level was approximately 0.55eV and 0.57eV lower than singlet energy levels of HD-1-mono and NCSU-10, respectively. Thus, triplet energy level of HD-1-mono is 0.1eV higher in energy than TiO_2 (-4.2 eV)[24] conduction band compared to

0.06eV of NCSU-10. Hence, because of the more free energy of the triplet level for HD-1-mono, more triplet electron injection was expected than that of NCSU-10.

2.3. Photovoltaic Device Characterizations

The photovoltaic performance of complexes HD-1-mono, NCSU-10 and N719 on nanocrystalline TiO_2 electrode was studied under standard AM 1.5 irradiation (100 mW cm^{-2}) using an electrolyte with a composition of 0.6 M dimethylpropyl-imidazolium iodide (DMPII), 0.05 M I_2, 0.1 M LiI in acetonitrile. Figure 4 shows the incident-photon-to-current efficiency conversion (IPCE) spectra for the cells fabricated with complexes HD-1-mono, NCSU-10, and N719, where the incident photon-to-current conversion efficiency (IPCE) values are plotted as a function of wavelength.

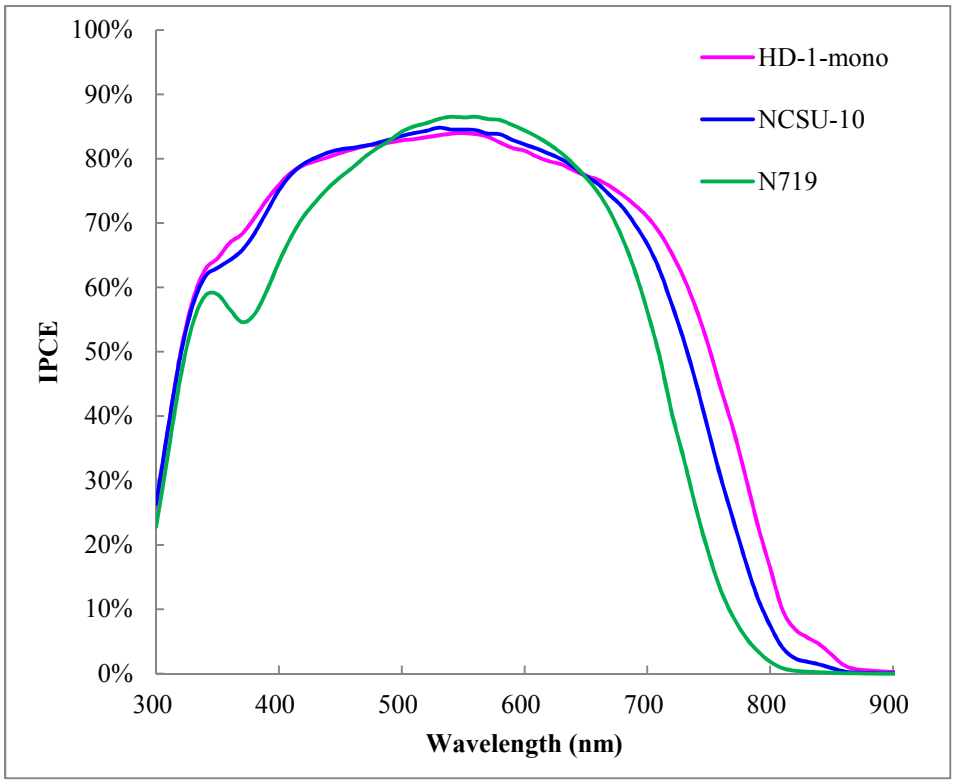

Figure 4. Photocurrent action spectra (IPCE) obtained with dyes HD-1-mono, NCSU-10 and N719 anchored on nanocrystalline TiO_2 film.

Figure 4 shows the impressive photocurrent response of carbazole based sensitizers HD-1-mono, NCSU-10. HD-1-mono outperformed the benchmark N719 in its photocurrent response owing to strong photon harvesting characteristics of carbazole based ancillary ligand. Presence of only one (mono) carbazole did not affect the IPCE negatively, compared to NCSU-10 (bis). In fact, HD-1-mono showed better response than NCSU-10 particularly in redder portion of the spectrum.

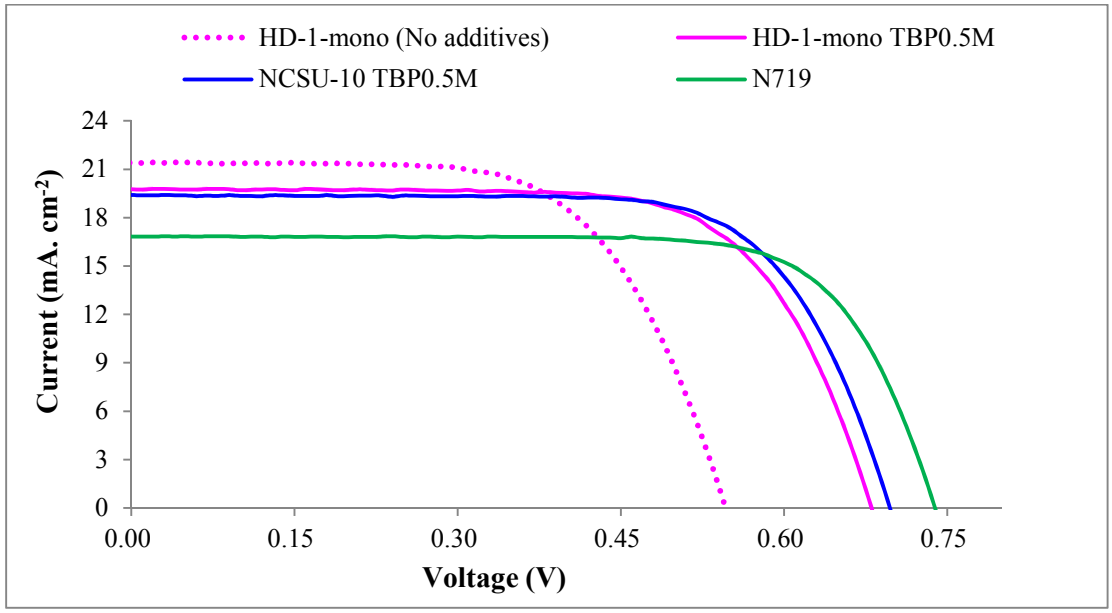

Figure 5. Photocurrent voltage characteristics of DSCs sensitized with the complexes HD-1-mono, NCSU-10 and N719 Electrolyte, 0.6 M DMPII, 0.1 M LiI, 0.05 I_2 in acetonitrile (AN), whereas TBP (tert-Butylpyridine) was added as an additive in the dye solution.

The photovoltaic parameters including the short-circuit photocurrent density (J_{sc}), open-circuit voltage (V_{oc}), fill factors (FF) and overall cell efficiencies (η) are summarized in Table 3.

Table 3. Photovoltaic characteristics of HD-1-mono, NCSU-10 and N719

Sensitizer	TBP (M)	J_{sc}(mA cm^{-2})	V_{oc} (V)	FF	η (%)
HD-1-mono	0.0	21.40	0.55	0.60	**7.06**
	0.5	19.76	0.68	0.694	**9.33**
NCSU-10	0.5	19.58	0.713	0.73	**10.19**
N719	0.5	16.85	0.749	0.739	**9.33**

[a]Conditions: sealed cells; coadsorbate, DCA 20 mM; photoelectrode, TiO_2 (15 µm thickness and 0.25 cm^2); electrolyte, 0.6 M DMPII, 0.1 M LiI, 0.05 I_2 in AN; irradiated light, AM 1. 5 solar light (100 mWcm^{-2}). J_{sc}, short-circuit photocurrent density; V_{oc}, open-circuit photovoltage; FF, fill factor; η, total power conversion efficiency.

The solar cell sensitized with HD-1-mono showed impressively higher short-circuit photocurrent density (J_{sc}) of 21.4 mA cm^{-2}, an open-circuit photovoltage (V_{oc}) of 0.55V, and a fill factor of 0.60, corresponding to an overall conversion efficiency (%η) of 7.06 without any additives. The J_{sc} of 21.4 mA cm^{-2}, which is 21% higher than J_{sc} of N719 is likely due to efficient photon harvesting and more energetically favorable electron injection into TiO_2 from the first excited triplet. An addition of 0.5M TBP resulted in J_{sc} of 19.76 mA cm^{-2}, V_{oc} of 0.68V and total conversion efficiency (%η) of 9.33 for HD-1-mono based solar cell. The impressive increase in V_{oc} and overall efficiency in the presence of TBP is likely due to the reduction of recombination between the injected electron and electrolyte at TiO_2–dye–electrolyte interfaces, owing to the formation of a protecting layer of TBP [5]. The upward shift in TiO_2 conduction band edge and an increase in electron lifetime were also reported to be caused by the presence of TBP [8]. Thus based on current-voltage results, it can be said that the attempted molecular modulation resulted in higher J_{sc} at the expense of decrease in photovoltage, which is most likely caused by dark current or recombination reactions.

Under similar conditions, HD-1-mono exhibited slightly lower *Voc* than NCSU-10, which contradicts with previous findings [20,21] of lower V_{oc} in case of bis ancillary ligand vs mono

analogs. Choi et al [20] and Jung et al [21] noticed a decrease in loading for bis compared to mono antenna based sensitizers. Our molecular design strategy circumvented this situation by employing highly efficient and small sized carbazole-based ancillary ligand.

2.4. Electrochemical Impedance spectroscopy characterization

Electrochemical impedance spectroscopy (EIS) is a key technique to study the electrical energy storage and dissipative properties of passive electrical systems. Impedance is different from resistance in that it also takes care of the dynamic processes such as relaxations related to dielectric and charge tranfer between heterogenous surfaces. In DSC, EIS is a powerful tool in charectrizing the interfacial charge transfer process at TiO_2/electrolyte and pt/electrolyte interfaces [22,29]. The EIS Nyquist and Bode plots for the DSCs based on HD-1-mono, NCSU-10 and N719 are shown in Figures 6 and 7, respectively. In EIS Nyquist plots, the intermediate frequncy range indicates the electron recombination resistance which was the highest for NCSU-10 compared to HD-1-mono and N719.

In Figure 7, the frequency response regime is in the range of 1-100 Hz, which is an indicative of the electron recombination between electrolyte and TiO_2 and is related to the electron lifetime in the CB of TiO_2 . The electron lifetime depends on the density of charge traps, which is ultimately related to V_{oc}. The middle-frequency peaks of the DSCs based on NCSU-10 and N719 were shifted to lower frequency relative to that of HD-1-mono, indicating a shorter recombination lifetime for the latter case, thus resulting in lower V_{oc} for HD-1-mono as compared to NCSU-10 and N719. EIS results clearly demonstrated qulitatively that in the case of HD-1-mono, the injected electrons are prone to recombine due to shorter lifetime in TiO_2 CB. Shorter TiO_2 life time for HD-1-mono can be attributed to the decrease in the hydrophobicity of the mono versus bis which resulted in decrease in the insulating propery of the dye towards

chrage recominations at TiO_2/ I_3^- interface compared to NCSU-10. Similar results of longer TiO_2 life time for carbazole based dyes were related to the density of alkyl chains present which block the access of I_3^- or cations to TiO_2 surface [30,31].

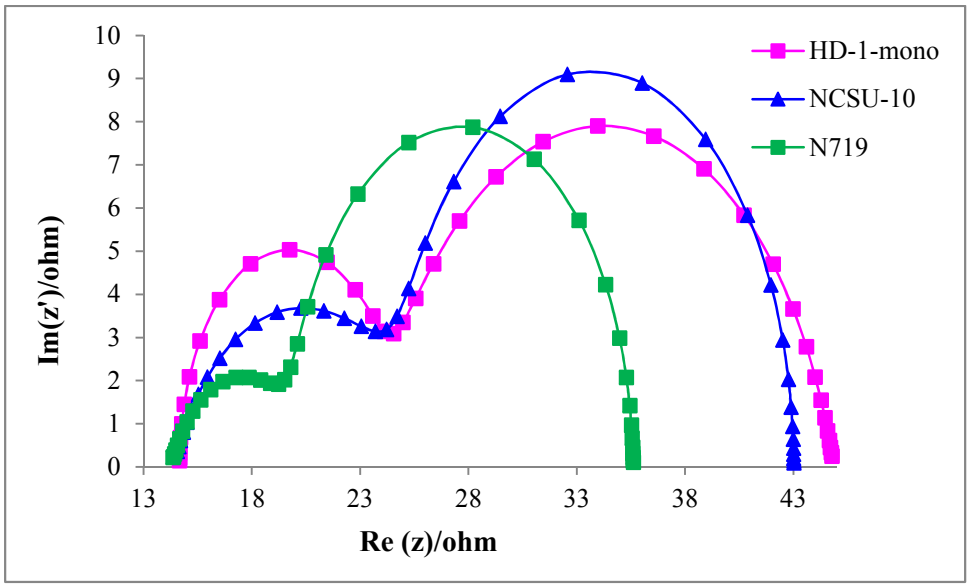

Figure 6. EIS Nyquist plots for DSCs sensitized with HD-1-mono, NCSU-10, and N719

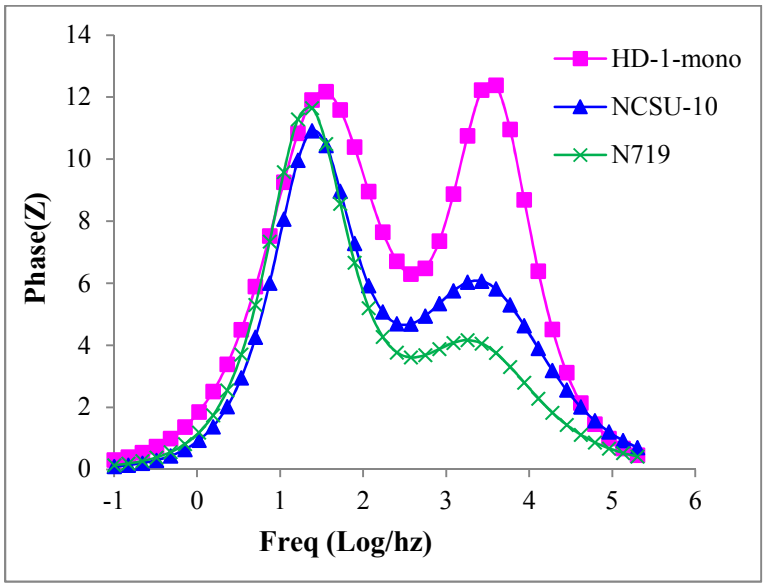

Figure 7. EIS Bode plots for DSCs sensitized with, HD-1-mono,NCSU-10 and N719

2.5. Time Correlated Single Photon Counting (TCSPC) Spectroscopy Measurements

TCSPC spectroscopy method was employed to study the excited state life time, and emission decay behavior of the dyes in solution and in cell form (DSC). Inset of Figure 8 shows the excited state decay behavior of the dyes in DMF. All of the decay curves were fitted with 2-exponential showing the multiexponental decay behavior having fast (shorter lifetime) and slow (longer lifetime) components. The relative amplitude of the fast component (B1) for HD-1-mono and NCSU-10 was substantially different from that of N719. The reported value of excited state lifetime for N719 in air saturated ethanol solution is 40ns [1], but in our case, it was 38ns in DMF. HD-1-mono and NCSU-10 exhibited the excited state life time of 85ns and 59ns, respectively as given in Table 4.

Table 4. Excited state lifetime in solution form

Sample Name	τ/ ns(T1)	τ/ ns (T2)
HD-1-mono	21 (*B1=32)	85 (B2=68)
NCSU-10	25 (B1=34)	59 (B2=66)
N719	0.1 (B1=3)	38 (B1=97)

*B denotes the relative amplitude of each component

However, when the decay behaviors were studied by TCSPC technique [32,33] on the complete DSC, the decay rate was in the following order HD-1-mono>NCSU-10>N719 as shown in Figure 8. The TCSPC decay behavior was consistent with the photocurrent response of dyes in DSC. Hence it can be postulated that faster decay is the result of reduced kinetic redundancy of excited state owing to optimized excited state lifetime as found by Durrant *et al* [33] which leads to

efficient electron injection, resulting in higher photocurrent for HD-1-mono, which is consistent with the shorter TiO_2 lifetime as found from EIS measurements.

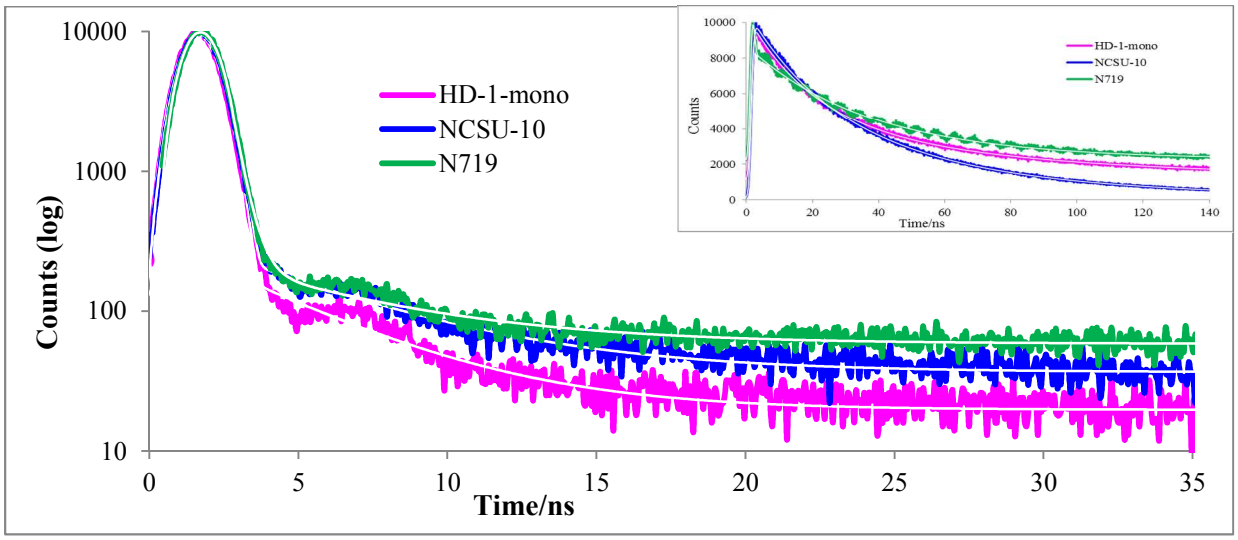

Figure 8. Excited state decay behaviors of HD-1-mono, NCSU-10 and N719 in complete cell, inset in solution dyes dissolved in DMF, studied with TCSPC method, smooth lines correspond to the fits of the experimental data after convolution with the instrument response.

2.6. Femtosecond Transient Absorption Spectroscopy Measurements

To understand the differences in J_{sc} and V_{oc} (Figure 5) of the devices as the function of electron-donor ancillary ligands, femtosecond transient absorption spectroscopy (TAS) was performed to understand the fundamental excited state dynamics by measuring the charge separation dynamics at the dye/TiO_2 interface. Figure 9(a) and (b) show the transient absorption spectra for these dyes at 0 ps and 500 ps as an example. It consists of ground state bleaching (GSB) with increased transmission above 2.0 eV (< 620nm) and the flat photo-induced absorption (PIA) band below 2.0 eV (> 620nm) for both samples.

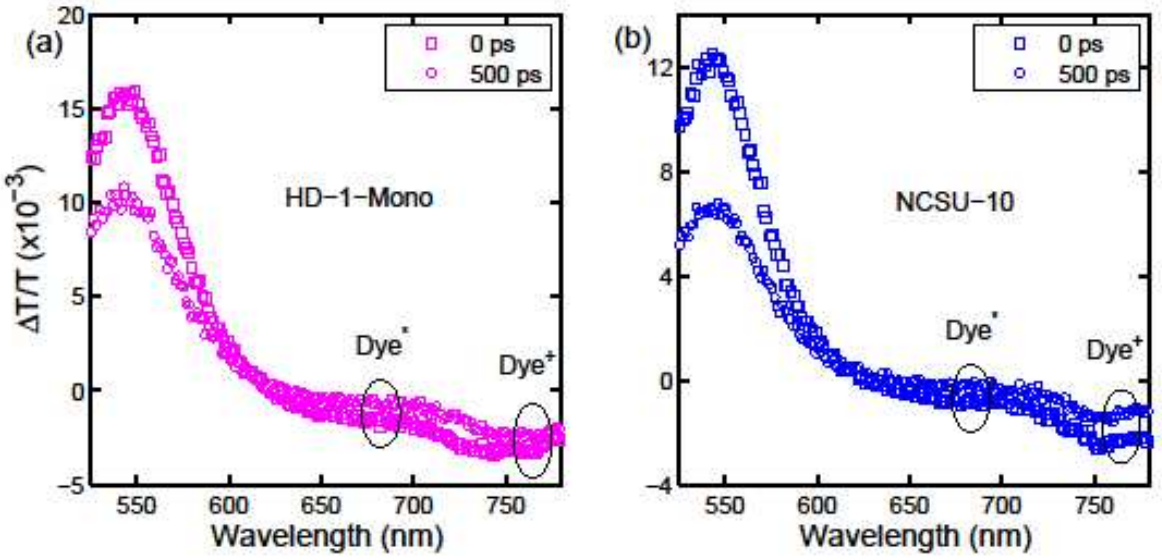

Figure 9. Transient absorption spectra at t=0 ps and t=500 ps of (a) HD-1-mono (b) NCSU-10 with electrolyte. Dye* and dye+ represent the majority of excited dye and oxidized dye population respectively.

Previous studies on similar Ru (II) based DSCs revealed that the PIA spectrum is sensitive to the charge separation dynamics as it probes the oxidized form of dye (dye^+), excited state dye (dye^*) and injected electrons into TiO_2 ($eTiO_2$) [34]. The PIA at 680 nm primarily reveals exciton population (dye^*) whereas at 770 nm, PIA reveals oxidized dye (dye^+) population [35]. Therefore comparison of the time evolution of these two spectral locations reveals a complementary picture of exciton lifetime and charge injection from the dye into TiO_2 [33,35-41].

Figure 10 shows the evolution of the PIA feature at 680nm and 770 nm, in samples without electrolyte. For both samples, the very fast rise at both 680 nm and 770 nm suggests an impulsive exciton creation and immediate charge injection. On the other hand, for both samples, 770nm data decays much slower compared to the 680 nm.

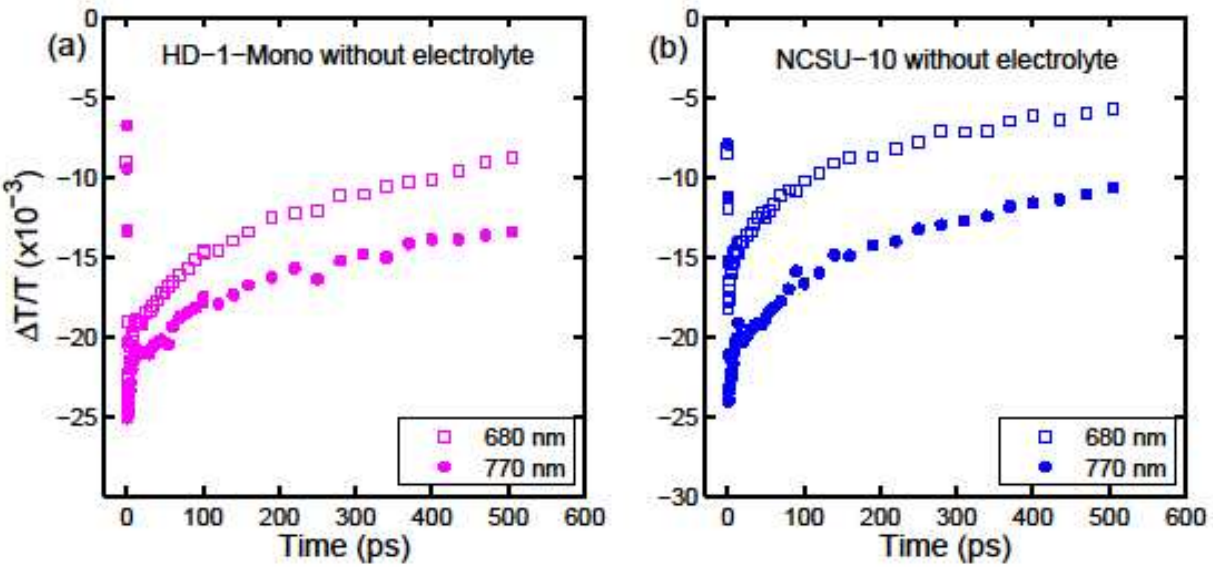

Figure 10. PIA decay dynamics of (a) HD-1-Mono and NCSU-10 without electrolyte (b) NCSU-10 without electrolyte. Colors are indicated in the legend.

Table 5 shows the comparison of the decay on two devices at 680 nm and 770 nm for each dye, HD-1-mono and NCSU-10. These data agree with the assessment that 680 nm probes primarily dye*, and 770 nm probes dye+. Because the dye* population decays through both recombination and charge injection into TiO_2 (Supplementary information 11S-12S).

Table 5. Comparison of decay of two devices for each dye, one at 680 nm and the other at 770 nm.

Sample Name	Wavelength (nm)	τ/ ps (T1)	τ/ ps (T2)	τ/ ps (T3)
HD-1-mono	680	3.5 ps (B1=22%)	89ps (B2=22%)	1014ps (B3=56%)
HD-1-mono	770	3.6ps (B1=17%)	136ps (B2=22 %)	2594ps (B3=61%)
NCSU-10	680	3.3 ps (B1=16%)	76 ps (B2=30%)	945 (B3=54%)
NCSU-10	770	4.3ps (B1=16%)	126ps (B2=27%)	1730 (B3=57%)

*B denotes the relative amplitude of each component.

The addition of electrolyte completely changes the dynamics. As shown in Figures 11 (a) and (b) the dynamics in 680 nm and 770 nm evolves in a different pace. In contrast to the sharp, fast rise and then slower decay at 680 nm, the dynamics at 770 nm exhibits a two-step growth process with sharp and slow components, which takes place over longer period of time. For NCSU-10, this slow rise saturates in the first 20ps. However, for HD-1-mono, it saturates at a later time of about 150 ps at greater amplitude. The saturation of growth of the slow component at 20 ps in NCSU-10 compared to that at 150 ps in HD-1-mono indicates that in HD-1-mono device, the charge injection continues for a longer time and is more efficient compared to that from NCSU-10[36].

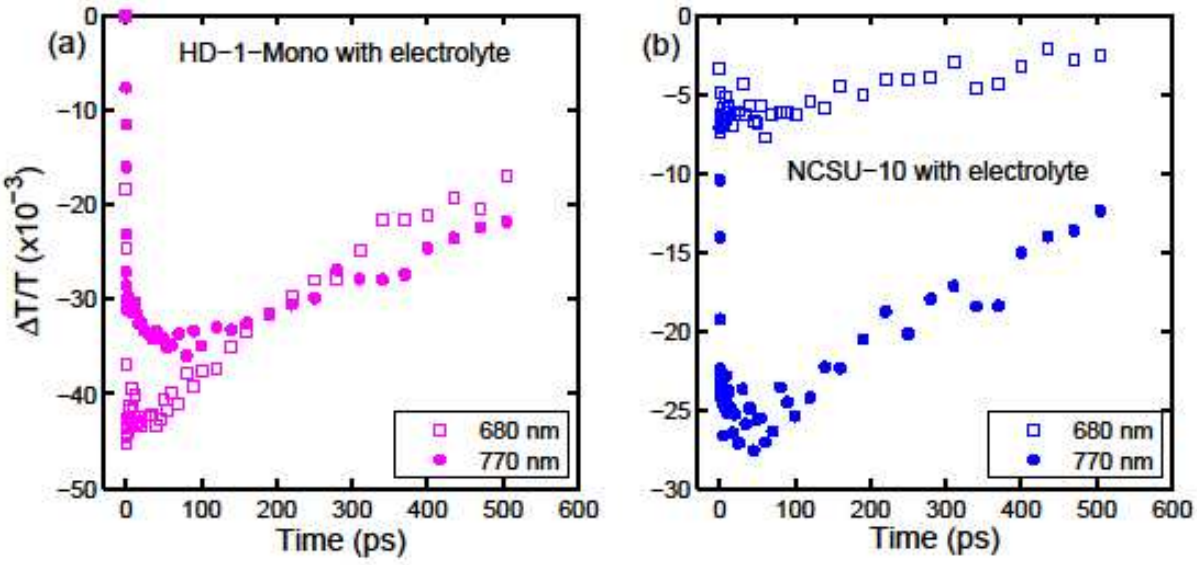

Figure 11. PIA decay dynamics of (a) HD-1-mono (b) NCSU-10 with electrolyte. Colors are indicated in the legend.

The comparison in these spectral evolutions in the two DSC structures clearly shows the difference in charge separation dynamics. In both samples, charge injection from the singlet states is very similar. With the addition of electrolyte, the Fermi level for the TiO_2 band and trap states shifts [33], which facilitates electron injection from the triplet state of the dyes. These data confirmed that triplet state injection is more efficient in HD-1-mono than in NCSU-10. In order to quantify the difference between the triplet state injections between the two dyes, we normalized the decay of 770 nm signal in the samples with and without the electrolyte. Since the electrolyte addition primarily enhances the injection from triplet state, we subtracted these two signals to find the relative increase in the triplet injection in both dyes. The results are displayed in Figure 12. The comparison of signal maxima in Figure 12 suggests 63% higher electron injection efficiency from the triplet state in HD-1-mono compared to NCSU-10. This increase is consistent with greater J_{sc} and observed for HD-1-mono. However, these data also suggest that not all of the injected charges are converted into current likely due to small negative free energy, which can be fine-tuned to enhance the efficiency of triplet injection.

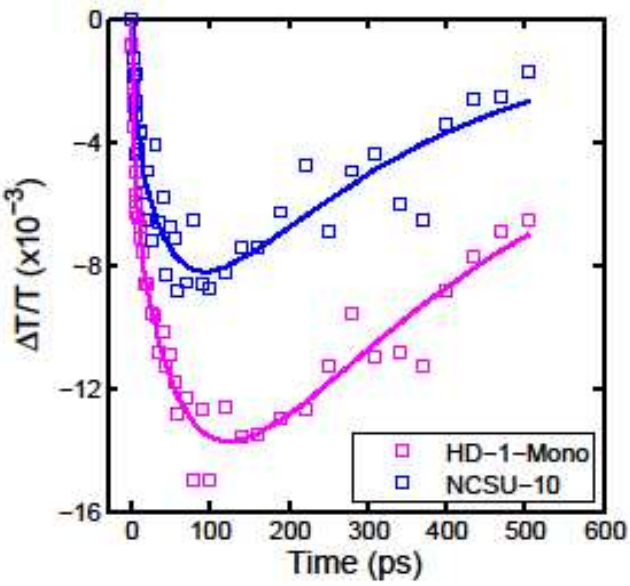

Figure 12. Comparison of triplet injection on HD-1-mono and NCSU-10. Solid lines refer to the fitting with three exponentials.

3. Conclusions

The attempted molecular modulation of bis (NCSU-10) to mono-carbazole (HD-1-mono) resulted in higher photocurrent response and favorable redox properties. Comparison of the photovoltaic, electrochemical and optical studies revealed that the number of ancillary ligands can have significant effect on the solar cell performance. Our findings showed that the V_{oc} of the mono versus bis contradict the previous findings of lower V_{oc} for bis analog, owing to superior photon harvesting and small molecular size of carbazole without sacrificing the solar to power conversion efficiency of solar cells. It was also found that HD-1-mono shows 63% more favored electron injection from triplet state compared to NCSU-10 as shown by femtosecond transient absorption spectroscopy experiments. Results from TCSPC of excited state decay rates were consistent with femtosecond TAS. EIS showed that HD-1-mono offers lower recombination resistance on TiO_2 surface compared to NCSU-10, and the injected electrons have shorter lifetime, resulting in enhanced recombination and lower V_{oc}. We believe this strategy will greatly help in the future design of efficient sensitizers both in terms of higher photocurrent and photovoltage for DSCs.

Supporting Information

Synthesis details, FT-IR, ^{1}H-NMR and CV graphs are given as Supporting Information.

Corresponding Author Ahmed El-Shafei, Ahmed_El-Shafei@ncsu.edu

REFERENCES

1. Nazeeruddin, M. K.; Zakeeruddin, S. M.; Humphry-Baker, R.; Jirousek, M.; Liska, P.; Vlachopoulos, N.; Shklover, V.; Fischer, C.; Gräetzel, M. *Inorg. Chem.* **1999***, 38*, 6298-6305.

2. Péchy, P.; Renouard, T.; Zakeeruddin, S. M.; Humphry-Baker, R.; Comte, P.; Liska, P.; Cevey, L.; Costa, E.; Shklover, V.; Spiccia, L.; Deacon, G. B.; Bignozzi, C. A.; Grätzel, M. *J. Am. Chem. Soc.* **2001***, 123*, 1613-1624.

3. Grätzel, C.; Zakeeruddin, S. M. *Materials Today* **2013***, 16*, 11-18.

4. - Zhang, S.; - Yang, X.; - Numata, Y.; - Han, L. - *Energy Environ. Sci.* , - 1443.

5. El-Shafei, A.; Hussain, M.; Atiq, A.; Islam, A.; Han, L. *J. Mater. Chem.* **2012***, 22*, 24048-24056.

6. O'Regan, B.; Grätzel, M. *Nature* **1991***, 353*, 737-740.

7. Hardin, B. E.; Snaith, H. J.; McGehee, M. D. *Nat Photon* **2012***, 6*, 162-169.

8. Hagfeldt, A.; Boschloo, G.; Sun, L.; Kloo, L.; Pettersson, H. *Chem. Rev.* **2010***, 110*, 6595-6663.

9. Grätzel, M. *Inorg. Chem.* **2005***, 44*, 6841-6851.

10. Mishra, A.; Fischer, M.; Bäuerle, P. *Angewandte Chemie International Edition* **2009***, 48*, 2474-2499.

11. Ahmad, S.; Guillen, E.; Kavan, L.; Grätzel, M.; Nazeeruddin, M. K. *Energy Environ. Sci.* **2013***, 6*, 3439-3466.

12. Yen, Y.; Chou, H.; Chen, Y.; Hsu, C.; Lin, J. T. *J. Mater. Chem.* **2012***, 22*, 8734-8747.

13. Zhang, S.; Yang, X.; Numata, Y.; Han, L. *Energy Environ. Sci.* **2013***, 6*, 1443-1464.

14. Nazeeruddin, M. K.; Splivallo, R.; Liska, P.; Comte, P.; Grätzel, M. *Chem. Commun.* **2003***, 0*, 1456-1457.

15. Grätzel, M. *J. Photochem. Photobiol. A.* **2004***, 164*, 3-14.

16. Hussain, M.; El-Shafei, A.; Islam, A.; Han, L. *Phys. Chem. Chem. Phys.* **2013***, 15*, 8401-8408.

17. Numata, Y.; Singh, S. P.; Islam, A.; Iwamura, M.; Imai, A.; Nozaki, K.; Han, L. *Advanced Functional Materials* **2012**, n/a-n/a.

18. Chiba, Y.; Islam, A.; Watanabe, Y.; Komiya, R.; Koide, N.; Han, L. *Japanese Journal of Applied Physics* **2006**, *45*, L638-L640.

19. Nazeeruddin, M. K.; De Angelis, F.; Fantacci, S.; Selloni, A.; Viscardi, G.; Liska, P.; Ito, S.; Takeru, B.; Grätzel, M. *J. Am. Chem. Soc.* **2005**, *127*, 16835-16847.

20. Choi, H.; Baik, C.; Kim, S.; Kang, M.; Xu, X.; Kang, H. S.; Kang, S. O.; Ko, J.; Nazeeruddin, M. K.; Grätzel, M. *New J. Chem.* **2008**, *32*, 2233-2237.

21. Jung, I.; Choi, H.; Lee, J. K.; Song, K. H.; Kang, S. O.; Ko, J. *Inorg. Chim. Acta* **2007**, *360*, 3518-3524.

22. El-Shafei, A.; Hussain, M.; Islam, A.; Han, L. *J. Mater. Chem. A* **2013**, *1*, 13679-13686.

23. Qu, P.; Meyer, G. J. *Langmuir* **2001**, *17*, 6720-6728.

24. Oskam, G.; Bergeron, B. V.; Meyer, G. J.; Searson, P. C. Cells. *J Phys Chem B* **2001**, *105*, 6867-6873.

25. De Angelis, F.; Fantacci, S.; Selloni, A.; Nazeeruddin, M. K.; Grätzel, M. *J. Phys. Chem. C* **2010**, *114*, 6054-6061.

26. Anderson, N. A.; Lian, T. *Coord. Chem. Rev.* **2004**, *248*, 1231-1246.

27. Ardo, S.; Meyer, G. J. *Chem. Soc. Rev.* **2009**, *38*, 115-164.

28. Prezhdo, O. V.; Duncan, W. R.; Prezhdo, V. V. Interface. *Acc. Chem. Res.* **2008**, *41*, 339-348.

29. Koide, N.; Islam, A.; Chiba, Y.; Han, L. *J. Photochem. Photobiol. A.* **2006**, *182*, 296-305.

30. Koumura, N.; Wang, Z.; Mori, S.; Miyashita, M.; Suzuki, E.; Hara, K. *J. Am. Chem. Soc.* **2006**, *128*, 14256-14257.

31. Miyashita, M.; Sunahara, K.; Nishikawa, T.; Uemura, Y.; Koumura, N.; Hara, K.; Mori, A.; Abe, T.; Suzuki, E.; Mori, S. *J. Am. Chem. Soc.* **2008**, *130*, 17874-17881.

32. Koops, S. E.; Durrant, J. R. *Inorg. Chim. Acta* **2008**, *361*, 663-670.

33. Haque, S. A.; Palomares, E.; Cho, B. M.; Green, A. N. M.; Hirata, N.; Klug, D. R.; Durrant, J. R. *J. Am. Chem. Soc.* **2005**, *127*, 3456-3462.

34. Juozapavicius, M.; Kaucikas, M.; van Thor, J. J.; O' Regan, B. C. *J. Phys. Chem. C* **2013**, *117*, 116-123.

35. Benko, G.; Kallioinen, J.; Korppi-Tommola, J.; Yartsev, A. P.; Sundstrom, V. *J. Am. Chem. Soc.* **2002***, 124*, 489-493.

36. Furube, A.; Wang, Z.; Sunahara, K.; Hara, K.; Katoh, R.; Tachiya, M. *J. Am. Chem. Soc.* **2010***, 132*, 6614-6615.

37. Katoh, R.; Furube, A.; Kasuya, M.; Fuke, N.; Koide, N.; Han, L. *J. Mater. Chem.* **2007***, 17*, 3190-3196.

38. Koops, S. E.; O' Regan, B. C.; Barnes, P. R. F.; Durrant, J. R. *J. Am. Chem. Soc.* **2009***, 131*, 4808-4818.

39. Sobus, J.; Burdziaski, G.; Karolczak, J.; Idogoras, J.; Anta. *Langmuir* **2014***, 30*, 2505-2512.

40. Tachibana, Y.; Moser, J. E.; Grätzel, M.; Klug, D. R.; Durrant, J. R. *J. Phys. Chem.* **1996***, 100*, 20056-20062.

41. Teuscher, J.; Dacoppet, J.; Punzi, A.; Zakeeruddin, S. M.; Moser, J.; Grätzel, M. *J. Phys. Chem. Lett.* **2012***, 3*, 3786-3790.

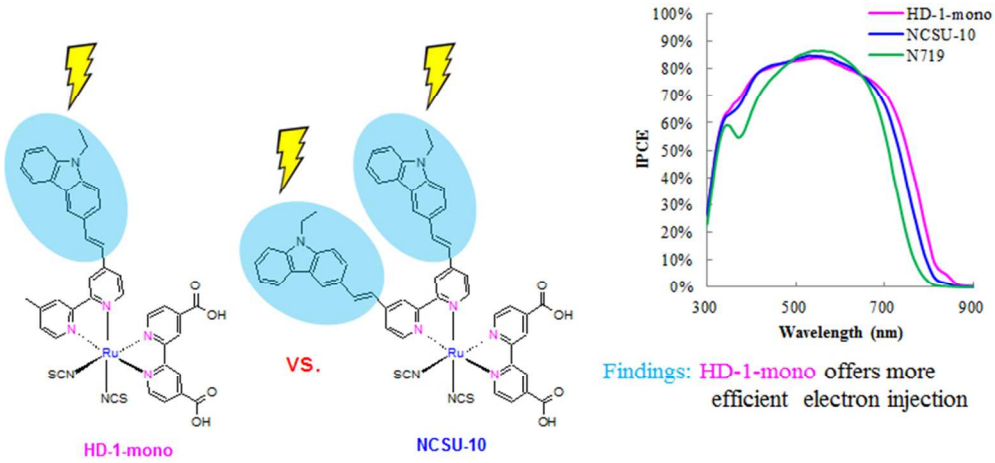

204x95mm (96 x 96 DPI)